APL Photonics

PERSPECTIVE | AUGUST 16 2024

Mid-infrared silicon photonics: From benchtop to real-world applications

Special Collection: Mid-IR Photonics

Colin J. Mitchell ; Tianhui Hu; Shiyu Sun ; Callum J. Stirling ; Milos Nedeljkovic; Anna C. Peacock ; Graham T. Reed; Goran Z. Mashanovich; David J. Rowe

APL Photonics 9, 080901 (2024)
https://doi.org/10.1063/5.0222890

Mid-infrared silicon photonics: From benchtop to real-world applications

Cite as: APL Photon. 9, 080901 (2024); doi: 10.1063/5.0222890
Submitted: 11 June 2024 • Accepted: 26 July 2024 •
Published Online: 16 August 2024

Colin J. Mitchell, Tianhui Hu, Shiyu Sun, Callum J. Stirling, Milos Nedeljkovic, Anna C. Peacock, Graham T. Reed, Goran Z. Mashanovich, and David J. Rowe[a)]

AFFILIATIONS

Optoelectronics Research Centre, University of Southampton, Southampton SO17 1BJ, United Kingdom

Note: This paper is part of the APL Photonics Special Topic on Mid-IR Photonics.
[a)]**Author to whom correspondence should be addressed:** d.rowe@soton.ac.uk. **Tel.:** +44 23 8059 7029

ABSTRACT

Silicon photonics is one of the most dynamic fields within photonics, and it has seen huge progress in the last 20 years, addressing applications in data centers, autonomous cars, and sensing. It is mostly focused on the telecommunications wavelength range (1.3 and 1.55 μm), where silicon becomes transparent. In this range, there are excellent light sources and photodetectors, as well as optical fibers operating with extremely low losses and dispersion. It is a technology that hugely benefits from the availability of complementary metal–oxide–semiconductor (CMOS) fabrication infrastructure and techniques used for microelectronics. Silicon and germanium, as another CMOS compatible group IV material, are transparent beyond the wavelength of 2 μm. The mid-IR wavelength range (2–20 μm) is of particular importance as it contains strong absorption signatures of many molecules. Therefore, Si- and Ge-based platforms open up the possibility of small and cost-effective sensing in the fingerprint region for medical and environmental monitoring. In this paper, we discuss the current mid-IR silicon photonics landscape, future directions, and potential applications of the field.

I. INTRODUCTION

Silicon photonics can utilize the unique absorption fingerprints of many molecules in the mid-IR wavelength range to realize compact, low power, and versatile sensors for a number of applications. Waveguide sensors based on absorption spectroscopy can find use in healthcare (e.g., blood analysis, breath analysis, hospital air quality monitoring, and imaging), environmental monitoring (e.g., gas detection and water and air quality), security and safety (e.g., detection of hazardous materials and gas leakage), industry (e.g., process control, maintenance, and surveillance), transport (emission monitoring and fuel control), or agriculture (e.g., quality of food). Silicon photonics chips can also significantly reduce the footprint of current astronomy setups and can utilize two atmospheric transmission windows (3–5 and 8–12 μm) for free space communications. Therefore, a strong motivation exists to develop silicon photonics mid-IR platforms, devices, and circuits for such a large application space.

It is not possible to cover all these applications or various reports on the development of mid-IR silicon photonic devices and circuits; hence, in this paper, we limit the discussion to two areas: medical diagnostics of liquid samples at longer mid-IR wavelengths (≈6–10 μm), where absorption features are complex and broad, and gas sensing at shorter wavelengths (3–5 μm), where absorption lines are narrow and well defined.

In both cases, the idea is to use waveguides with optimized lengths for light–analyte interaction. Not only can the interaction length be controlled, but also the fraction of light that interacts with the analyte (via the waveguide's evanescent field). These are the main advantages compared to Attenuated Total Reflectance-Fourier Transform Infrared (ATR-FTIR) spectroscopy, which has been extensively used, particularly within analytical chemistry, which uses one or several bounces of light at a transparent crystal surface.

Silicon and germanium have wide mid-IR transparencies and benefit from existing silicon fabrication infrastructure. They offer high refractive index contrast waveguide platforms for small footprint circuits, together with the potential for electronic–photonic integration. Si and Ge also have strong nonlinear effects.

However, the realization of SiPh absorption spectroscopy sensors brings several challenges:

- Typical claddings used in the near-IR (e.g., SiO_2) show very strong absorption at longer wavelengths, so new material platforms are needed in the mid-IR.
- The mid-IR is a very large wavelength range, and there may not be a single dominant material platform comparable to silicon-on-insulator (SOI) in the near-IR.
- Strong water absorption can mask useful absorption features; in some applications, it is necessary to minimize light–water interaction.
- The realization of mid-IR sources and their integration with Si and Ge material platforms is not trivial.
- Mid-IR detectors have inferior performance compared to their near-IR counterparts.
- To achieve low limits of detection, preconcentration techniques may be required.
- Packaging is already challenging in the near-IR, and it is even more complicated in the mid-IR due to using different materials or fragile optical fibers.

In this paper, state-of-the-art technologies are discussed, and the challenges and routes to provide mature circuits suitable for real-world systems are addressed. We write about applications that require relatively narrow spectral bands of operation and, as a more exploratory area, about medical applications (e.g., cancer detection), which require much wider spectral bands. This paper is organized as follows: we first describe the components that are needed for a hypothetical sensor in order to frame the discussion in subsequent sections. We write about applications, then present various Si- and Ge-based material platforms; we then discuss mid-IR sources, detectors, and modulators before reviewing nonlinear effects; this is followed by perspectives and challenges of integration; and finally, we give some conclusions. Throughout, we entirely restrict discussion to silicon and germanium based photonic integrated circuit (PIC) platforms. Since the indirect bandgaps of silicon and germanium make them highly inefficient for lasing, in the sources and detectors sections, we explore how other materials could be introduced into these PIC platforms to compensate for this shortcoming.

II. COMPONENTS OF A HYPOTHETICAL SENSOR

Figure 1 shows a schematic of a hypothetical integrated sensor chip and the major components. The diagram shows break points where components could be integrated on a separate chip or taken off-chip entirely, necessitating coupling to the transducer chip.

A sensor requires a source, a transducer, and a detector. The transducer is the most fundamental component and, for an integrated silicon photonics sensor, uses a waveguide or waveguide-coupled resonator to interrogate a sample brought into its evanescent field. Sensing is performed by comparing the difference in propagation through the photonic circuit depending on the presence of the material under test. The interaction of light with an analyte can be controlled by only exposing a predefined length of waveguide to the analyte by etching a photolithographically defined area in the waveguide cladding. The interaction can also be controlled by waveguide design, for example, by modifying the width and etch depth of a rib waveguide to maximize the fraction of the evanescent field outside of the waveguide core and substrate. This can be further increased by suspending the waveguide, which is particularly convenient for gas sensing so that the evanescent field underneath the waveguide and between the lateral subwavelength claddings can also interact with the analyte. The transducer can be further modified

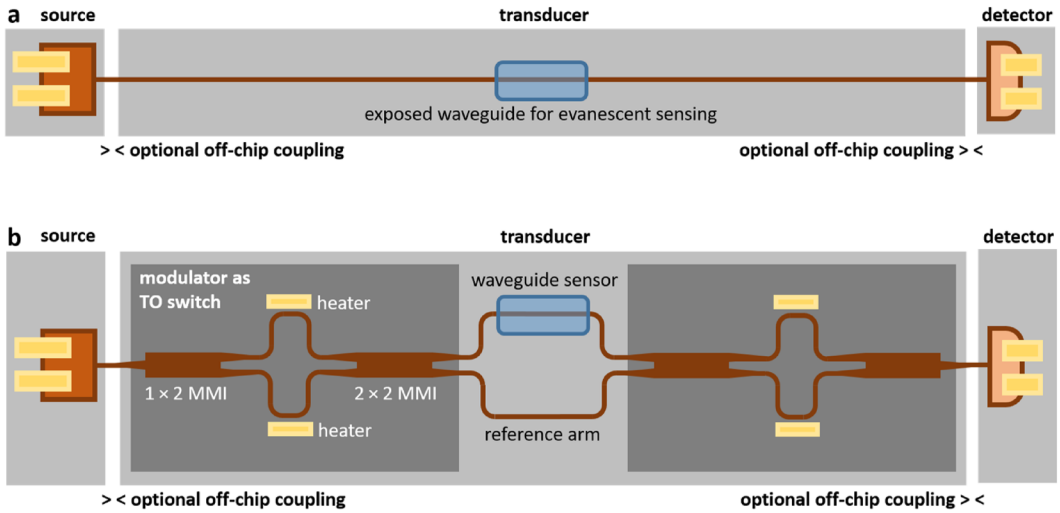

FIG. 1. Example schematics for integrated silicon photonics sensors, including breaks where off-chip coupling would be required if the source or detector were not integrated on chip. (a) Shows the minimum number of components, including a source, detector, and window etched in the cladding to expose a length of waveguide to implement the evanescent sensing transducer; and (b) includes two modulators used to implement thermo-optic (TO) switches to continuously switch between a sensor arm and a reference arm. The heaters modulate the phase difference between the two arms, enabling light to be routed along different paths through the 1 × 2 switches.

by functionalization, where a target species is bound to the sensor surface to increase its interaction with the evanescent field, or by coatings that exclude interferents such as water.

One or both of the source and detector can be integrated on-chip or coupled off-chip. They could also be integrated onto a separate chip and subsequently coupled to it. Typical coupling structures can be divided into grating and end-fire coupling. Grating coupling requires a structure to be etched into the waveguide, so a fraction of the optical power is diffracted into or out of the waveguide. End-fire requires light to be coupled to a prepared end facet. Both grating and end-fire coupling can be implemented with optical fibers, ideally mode-matched to the grating or end facet to maximize coupling efficiency, and free space, where an objective is used to focus light to a suitable spot size on the grating or end facet.

The decision of whether to integrate a source or detector onto a transducer chip is application specific. For example, medical sensors cannot be reused in clinical practice because of the risk of cross-contamination, so the transducer would typically be disposable. In this situation, the integration of a laser source onto the same chip as the transducer would be prohibitively expensive and ecologically wasteful. However, it may be possible to implement a detector much more simply and cheaply than a laser. The transducer and detector could be integrated on the same chip, so only one coupling interface needs to be aligned (i.e., between the source and transducer). Conversely, an atmospheric gas sensor deployed on a drone would not need to be disposable and would benefit greatly from the reduced footprint and improved vibration tolerance associated with integration.

Additional components can be integrated. For example, modulation strategies can greatly improve the signal-to-noise ratio (SNR) of absorption measurements, so integrated modulators are highly desirable for silicon photonics sensor chips. Similar components can be used to implement thermo-optic switches to choose between a sensor arm and a reference arm, as shown in Fig. 1(b). Taking the ratio of the transmissions through two arms is an effective referencing strategy for reducing time-dependent measurement errors such as drift or fluctuations in source power. This enables superior performance to the simpler device shown in Fig. 1(a), which requires sequential reference and sensing measurements. An alternative scenario would be to split light between the sensor and reference arms and use a pair of detectors to continuously measure the signals of both of them.

III. APPLICATIONS: ENVIRONMENTAL SENSING

Environmental sensing covers a broad range of applications, including greenhouse gas and contamination detection. These occur in both the gas phase, such as analyzing industrial emissions for greenhouse and toxic gases, and the liquid phase, such as deep-sea dissolved greenhouse gases and river water pollutants.

There are also plentiful mid-IR imaging applications such as heat emission monitoring for building control, military purposes such as the detection and identification of heat signatures, or FTIR astronomy using the James Webb Space Telescope. However, these are beyond the scope of this perspective.

A. Current state-of-the-art in silicon photonics for mid-IR environmental sensing

The major greenhouse gases are carbon dioxide (CO_2), methane (CH_4), and nitrous oxide (N_2O). Of these, CO_2 occurs at the highest concentration in the atmosphere and N_2O at the lowest. CO_2 also has very strong absorption features compared to the other two gases, but these absorptions are at wavelengths around 4.2 μm. Conversely, CH_4 has absorptions at lower wavelengths, accessible using the silicon-on-insulator platform, so the technology has correspondingly better performance. This shows how CO_2 is not necessarily the simplest gas to detect because the limit of detection for each gas is a combination of its concentration, its absorption intensity, and the sensitivity of the detection technology at the relevant wavelength.

The first example of an integrated silicon photonics sensor for greenhouse gas emissions used the SOI platform to detect CH_4 in the near-infrared region at $\lambda = 1650$ nm.[1] The limit of detection was shown to be <100 parts per million by volume (ppmv). Similarly, the limit of detection of acetylene, an extremely flammable fuel, was shown to be 7 ppmv at $\lambda = 2566$ nm using a suspended tantalum pentoxide waveguide platform.[2] A later paper from the same group demonstrated the mid-IR detection of CH_4 at $\lambda = 3270.4$ nm with a limit of detection of 0.3 ppmv using a Si slot waveguide with an integrated gas cell.[3] Another example of mid-IR gas sensing is where a suspended silicon waveguide with a metamaterial-assisted comb structure was used to detect acetone at concentrations of 2.5 ppm using a wavelength of 7.33 μm.[4]

B. Prospects in silicon photonics for mid-IR environmental sensing

Environmental sensing is notable for its harsh conditions, meaning that the sensing technology has to be correspondingly robust. For example, underwater deployment to significant depths requires the capability to operate at high pressure, while operation in space requires radiation hardness. These factors have important implications for fabrication, particularly for packaging.

The mid-IR absorption of methane is more than 100 times stronger than its absorption bands in the near-infrared. Although this has not yet been demonstrated in the literature, the growing maturity of the material platforms at longer wavelengths suggests that significantly higher sensitivity could be achieved for methane detection if comparable waveguide loss and detector performance were available.

Environmental sensors can generally be reused. For example, the transducer of an atmospheric gas sensor will not become fouled as readily as a blood sensor. Referring to Fig. 1, this means that the source and detector are appropriate for complete on-chip integration because the transducer does not have to be disposable.

IV. APPLICATIONS: BIOMEDICAL SENSING

Mid-IR sensing for biomedical applications can be divided into two broad categories: those that detect a particular analyte, such as a protein or a drug, and those that apply machine learning or other big data methods to entire mid-IR spectra to investigate system-level changes. The former are typically narrowband, and the latter are typically wideband.

A. Current state-of-the-art in silicon photonics for mid-IR biomedical sensing

Cocaine sensing for illicit drug monitoring has been demonstrated using single-wavelength measurements at $\lambda = 5.8$ μm using the germanium-on-silicon (GOS) platform.[5] This was used to detect 500 mg/l concentrations of cocaine in spiked samples of human saliva, showing that this method could find application in overdose detection in emergency medicine.[6] Protein sensing, which has implications for many pathologies, such as prostate cancer screening through the measurement of prostate specific antigens, has also been demonstrated using the GOS platform.[7,8] There is a far wider range of applications demonstrated using FTIR spectroscopy. These include cancer diagnosis for brain,[9] pancreatic,[10] and lung[11] cancers and microbiological diagnosis for pathogens, including SARS-CoV-2[12] and malaria.[13] However, none of these are routinely used in clinical practice.

B. Prospects in silicon photonics for mid-IR biomedical sensing

Existing research on cancer diagnostics shows retrospective prediction using samples from symptomatic patients who have already received a diagnosis. The clinical utility would be vastly improved by prospective studies. This means that future work should analyze samples from asymptomatic patients, i.e., drawn from a risk-based cohort, before they have a confirmed diagnosis. Being able to detect malignancies before the onset of related symptoms would potentially allow us to detect cancer much earlier and, therefore, so improve treatment outcomes. If the measurement could be performed using a microsample, such as a fingerprick of blood, then this method could become part of a routine healthcare check-up. From a spectroscopy perspective, protein sensing has been demonstrated using a similar wavelength region, but such tests have not been demonstrated using integrated photonics. As such, they remain specialist laboratory techniques that are unlikely to find their way into routine clinical practice.

From a practical perspective, integrated silicon photonic sensors have strong potential for translating mid-IR spectroscopy into clinical practice. They have several key advantages over benchtop FTIR spectroscopy. First, the majority of the bandwidth of an FTIR spectrometer covers spectral regions containing no information. An integrated silicon photonics sensor can have a much higher power spectral density by using a source with a narrower bandwidth and significantly higher intensity within the spectral region of interest. Second, photonic circuits can be used to implement self-referencing strategies to cancel out any potential background absorptions or power fluctuations in the source [cf. Fig. 1(b)], meaning measurements can be taken continuously. Conversely, an FTIR spectrometer requires a reference measurement to be taken between each sample measurement, which is both slower and cannot account for temporal changes in source intensity or background variation. Third, integration means there are no bulky or fragile free-space optics that need to be kept in alignment. Fourth, confining light entirely within a photonic circuit except for its sample interaction means there is no need to remove water vapor or CO_2 from the beam path. This removes the need for a nitrogen supply to purge the instrument, making implementation much simpler in a clinical setting. Fifth, the potential for a low-cost sensor chip to be disposed of without carrying a source or detector removes the requirement for the operator to clean and sterilize the optical sensing surface. Sixth, with suitable electronic and microfluidic integration, the sample could be delivered to a sensor and characterized using an automated routine that does not require the user to be trained in sample preparation. The device could potentially show the relevant metrics to the attending clinician or report back to a secure repository. These points illustrate how an integrated silicon photonic sensor could be smaller, more sensitive, and more robust than existing technology while being operable by a non-expert user. A schematic of a hypothetical device is shown in Fig. 2, where a disposable chip including a grating-coupled photonic sensor with integrated microfluidics is inserted into an instrument for mid-IR characterization.

A crucial aspect of mid-IR sensing using integrated photonics is spectral bandwidth. In order to port cancer detection to an integrated photonics platform, a far greater range of usable bandwidth is required from the technology. For example, FTIR brain cancer detection requires measurements over the 2.5–10 μm wavelength range.[9] FTIR spectroscopy is a powerful technique, but it has shortcomings that limit its widespread deployment. FTIR spectrometers are essentially free-space optical systems packaged in a box. Smaller, more portable options tend to not have cooled detectors or nitrogen-purged beam paths to exclude water vapor and have correspondingly worse performance. Integrated silicon photonics has the potential to address many of the issues related to cost, robustness, and alignment sensitivity if the material platform and components can perform adequately over a sufficiently wide spectral range.

Single wavelength measurements, such as those used to demonstrate cocaine detection in saliva,[5] are unlikely to find utility in real-world measurements because of the lack of specificity. For example, baseline drift would appear to be the same as a change in cocaine concentration. In practice, this could be counteracted by using a differential measurement with at least one other wavelength in the spectrum that has been shown to not vary with the presence of cocaine or other interferents. In practice, local zeros can often be found near drug peaks in the fingerprint region, meaning that such a differential measurement could still be implemented with a narrowband source.

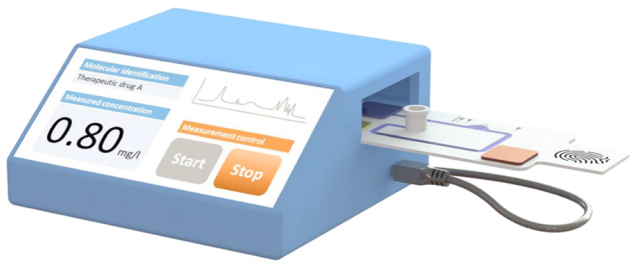

FIG. 2. Schematic showing a disposable integrated microfluidic-photonics chip being inserted into a spectroscopy instrument. This would contain a grating-coupled source and detector with readout electronics. It would also contain sufficient computational power to extract the concentration of a particular analyte from the spectra using a preprogrammed regression routine and then display the result.

V. MID-IR MATERIAL PLATFORMS

A. Current state-of-the-art in mid-IR material platforms

The properties of Si- and Ge-based material platforms have meant they have received significant interest for use in mid-infrared (mid-IR) integrated photonic devices; in particular, the broad transparencies and high refractive indices of silicon and germanium make them strong candidate materials for waveguide circuits.[14,15] In addition, these materials are compatible with complementary metal–oxide–semiconductor (CMOS) fabrication and consequently offer a pathway toward scalable manufacturing. Figure 3 shows the best results for propagation loss for Si- and Ge-based waveguide platforms across the mid-IR range of 2–12 μm. Note that for some waveguide demonstrations, multiple discontinuous points have been selected to demonstrate their operation within different spectral regions.

For shorter mid-IR wavelengths, silicon is transparent up to wavelengths of 8 μm and, with a refractive index of ≈3.4, can be used to make compact photonic devices. Silicon-based waveguides have been demonstrated at mid-IR wavelengths with various claddings, including silicon-on-insulator (SOI),[16–22] silicon-on-sapphire (SOS),[23,24] and silicon-on-silicon nitride (SON).[25] However, all these claddings absorb at wavelengths below the upper transparency limit of silicon, thereby restricting the transparency range of the respective platforms. Silicon dioxide, sapphire, and silicon nitride absorb above 4, 5, and 6.7 μm, respectively; in Fig. 3, it is evident that the SOI, SOS, and SON platforms are not used far beyond these upper limits. To facilitate the exploitation of the full silicon transparency, the waveguide can be undercut to remove the lower cladding and create a suspended membrane waveguide. Such suspended silicon platforms[4,26–30] have been demonstrated with low propagation losses up to 8 μm and are particularly useful for sensing applications as the mode can interact with an analyte both above and below the waveguide.

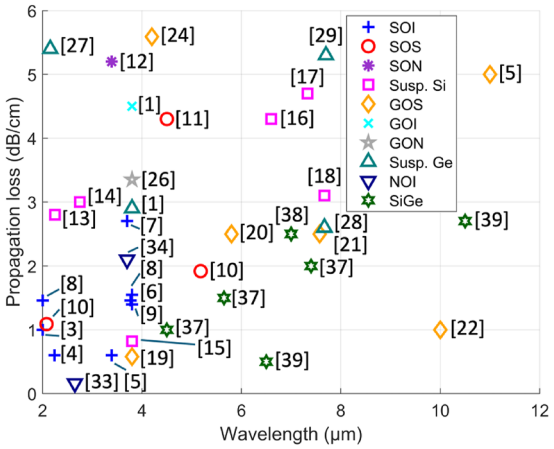

FIG. 3. Experimental demonstrations of different group IV waveguide platforms. Each datum is labeled with the reference from which it was taken. The data are available in its entirety in Table 1 of the supplementary material.

The GOS platform can be used to access the longwave mid-IR range due to its increased IR transparency up to 15 μm.[31–36] GOS waveguides have been shown to have reasonably low loss (less than 5 dB/cm) over different wavelengths within the range of 3.8–11.5 μm by several authors, making them suitable for various mid-IR applications. However, various authors have observed losses with a spectral dependence in the long-wavelength range,[33,34,37] resulting from a variety of factors, including modal overlap with the underlying silicon and consequent absorption; threading dislocations at the silicon–germanium interface; vibrations of interstitial oxygen in Czochralski-grown silicon; and free carrier absorption (FCA) caused by background doping.

While having decreased transparency, platforms such as germanium-on-insulator (GOI)[15] or germanium-on-silicon nitride (GON)[38] have under-claddings with lower refractive indices. In these platforms, the larger refractive index contrast between the waveguide core and cladding will increase the confinement of the mode within the germanium. This could reduce excess losses from modal interaction with the cladding and the threading dislocations, although these waveguides have not been demonstrated at longer wavelengths. Alternatively, as with silicon-based platforms, the underlying cladding can be removed to suspend the germanium waveguide.[15,39–41] However, while these suspended germanium waveguides have been characterized with comparable loss at 7.7 μm (see Fig. 3), they are yet to be demonstrated beyond the transparency range of silicon. It is in the wavelength range of 8–10 μm that the additional losses in the GOS platform become evident, so the suspended germanium waveguides cannot yet be fairly contrasted for any benefit.

Silicon nitride is widely transparent from visible wavelengths up to 6.7 μm, making it suitable for many shortwave mid-IR gas sensing applications. Silicon nitride-on-insulator (NOI) waveguides have been shown to have a low loss of up to 3.7 μm,[42,43] beyond which they have limited transparency due to silicon dioxide absorption such as SOI. However, the refractive index of silicon nitride (≈2.0) is significantly lower than that of silicon (≈3.4), and thus, the evanescent field of an NOI waveguide mode is comparatively larger, which has been used advantageously for gas sensing applications.[44]

For longer wavelengths, silicon–germanium (SiGe) alloys have been shown to have low losses across much of the mid-IR range.[45–48] Apart from the structure reported in Ref. 45, which consists of a step-index SiGe waveguide on silicon, this platform utilizes material growth from a pure silicon substrate up to germanium-rich (or pure) material near the surface. When the waveguide is etched, the mode will be confined to the germanium-rich region. These waveguides are generally thick (≈4–10 μm[46–48]) and have broadband performance. However, they also share some of the additional losses observed in the GOS platform, including free carrier absorption and vibration of interstitial oxygen; the reader is referred to Ref. 48 for a full analysis of the loss mechanisms in these waveguides. For sensing applications, platforms that have a very strong confinement of the optical mode within the waveguide will have reduced sensitivity. This is a drawback for most germanium-based waveguides due to the large refractive index of germanium (≈4.0). However, for the thick SiGe waveguides, sensing experiments have been used to derive modal power fractions in the analyte below 1%.[49] In contrast, a recent on-chip methane sensing demonstration

used a slot SOI waveguide with a modal confinement of 69% in the analyte.[3]

B. Prospects for mid-IR material platforms

As the platforms for mid-IR silicon photonics become more established and mature, the attention of the field is turning to building these devices into practical systems for real world use. While some may consider this solely a packaging or integration issue, there is significant scope for advancing the fundamental device design to this end.

In our opinion, SOI and NOI are the best material platforms for sensing applications at wavelengths up to 4 μm because of their low loss, robustness, and well-developed fabrication processes. For low analyte absorption applications such as gas sensing, suspended silicon could be more appropriate because of its potentially higher sensing figure of merit (evanescent field fraction/propagation loss) compared to SOI and NOI up to wavelengths of 4 μm and GOS or SiGe up to 8 μm. The evanescent field enhancement of suspended silicon can also be improved by using either a slot[26] or sub-wavelength grating[4] in the suspended design. However, to our knowledge, there are no current demonstrations of these devices outside of the laboratory environment. There consequently remains uncertainty around the robustness of the suspended membrane waveguides in practical scenarios. A real-world sensor may have to endure shocks or vibrations, particularly when operating in environmental or industrial monitoring applications. Similar membrane devices, such as microelectromechanical systems (MEMS), are known to exhibit significant fragility to shock,[50] so it can be reasonably expected to be the same for these devices. Consequently, the suspended waveguide design must be considered holistically for future devices; the waveguide must be optimized for the mechanical response of the structure as well as the optical response, with a common figure of merit. For applications in the wavelength range of 4–8 μm with strong analyte absorption compared to the waveguide propagation loss, material platforms with higher waveguide confinement, such as GOS or SiGe, are most appropriate.

For long wavelength applications above 8 μm, we expect germanium-based platforms to become the dominant approach due to their broad transparency, ease of fabrication, and reasonable evanescent field (in comparison to SiGe waveguides). However, in addition to the loss mechanisms highlighted above, the critical flaw of germanium is its highly water-soluble oxide. The exposure of the surface of a device to an aqueous environment or even environmental humidity is damaging to the device. For germanium-based platforms to be used in real-world scenarios, the device surface must be passivated to prevent oxidation without significantly increasing loss. Furthermore, an optically isolating cladding layer would facilitate both the protection of the device and integration with a larger system. The cladding could be used to lithographically control the interaction length through sensing windows or enable the bonding of other system components, such as microfluidics.[5] However, no CMOS-compatible material with extended mid-IR transparency has been established in the literature. Moreover, for some applications, it may be beneficial to use water exclusion and analyte enrichment layers even within the interaction regions, but at the cost of increased propagation loss.[51] Further research in this area is required, as it could become a critical requirement for applications in aqueous environments.

VI. SOURCES

The broad range of wavelengths required to cover the desired spectra could be spanned by thermal emitters. However, coupling such sources into a waveguide system has two main drawbacks. First, the limited amount of power that can be coupled from an incoherent source into a single mode is low at any given wavelength. Low spectral density causes a correspondingly poor signal-to-noise ratio for sensing applications. Second, most of the power is outside of the spectral regions of interest and would act to heat an integrated device. This could lead to thermal effects such as strain and misalignment of bonded structures. Supercontinuum (SC) sources and other nonlinear sources such as frequency combs can emit into single modes over very broad ranges and solve the single mode waveguide coupling issue, but they would still suffer from low power spectral density. A higher SNR could be achieved by using lasers that are tunable across the required wavelength range, provided that the tuning range is sufficiently wide for the application.

Mid-IR lasing can be realized in a number of ways, but the most developed and commonly used method is to engineer the material properties of compound semiconductors by varying composition, as with near-IR lasers. However, this alone does not give access to the full mid-IR range due to the intrinsic bandgap properties of the materials involved. The design of heterostructures allows for intersubband transitions within a quantum well to access an extended range of discrete energy levels covering the mid-IR range and beyond to the far-IR and terahertz ranges. The quantum cascade laser (QCL) is such a device and was first proposed in 1971[52] and realized in 1994.[53]

QCLs are unipolar devices that most commonly use energy transitions of electrons within the conduction band as opposed to exploiting electron–hole recombination, as in conventional lasers. After relaxing to a lower discrete energy level and emitting a photon, the electrons can tunnel from one quantum well to the next before relaxing again to emit another photon. As the process repeats many times, an individual electron cascades through the structure and emits many photons. This gives a range of photon energies that are not accessible via conventional band-to-band (interband) lasers. However, QCLs require efficient thermal management of the heat generated through the tunneling process and relatively high electrical power consumption. Good heatsinking and design enable continuous wave (CW) operation at room temperature.

The interband cascade laser (ICL), first proposed in 1994,[54] gives lasing at lower electrical power due to the interband transition of a type-II semiconductor where electrons and holes combine. An electron can cascade through an ICL in a similar way to a QCL because different layers of the ICL are designed so that the valence band of one layer overlaps with the conduction band of the next, enabling electrons to tunnel between them. The interband transition means that ICL devices are more suited to operation at shorter wavelengths in the mid-IR, with CW operation in the range of ≈3–6 μm. The interband transition also allows vertical emission, unlike QCL devices, where polarization selection rules prohibit surface emission without using an alternative approach such as an integrated

reflector.[55] This allows the fabrication of vertical cavity surface emitting laser (VCSEL) structures with ICL material to form IC-VCSEL devices. This enables an integration strategy where a laser source could directly couple to a grating without the use of a reflecting surface or additional angled mount. This could be achieved either by a support structure with different heights or with the IC-VCSEL bonded parallel to the substrate above a grating-coupled waveguide grown on an etched angled surface to match the optimum efficiency of the grating.[56]

QCLs and ICLs can emit a single wavelength in a similar way to more conventional interband lasers using etched Bragg gratings. These form either distributed feedback (DFB) or distributed Bragg reflector (DBR) lasers, which have relative merits in stability and tunability. Multiple etched Bragg gratings can be used to generate multiple wavelengths from the same material, which could then be coupled into a single waveguide as with a communications system. The lasers could be produced on separate chips or within a single laser bar by changing the grating design of adjacent lasers. Multiple laser wavelengths allow for fingerprint detection by detecting relative changes in multiple peaks. Multiple wavelength operation can also be achieved with a single laser by layering different active regions on top of each other. In this way, multiple wavelengths emitting from the same cavity can be produced entirely from the design of the heterostructure. These options allow a large degree of flexibility for selecting application-specific wavelengths through design rather than altering the intrinsic material properties.

Another important source design consideration is the method of wavelength selection, which will be application dependent. One option is to have multiple stable wavelengths, either closely spaced in energy across a single absorption feature or more widely spaced across several features. The latter would suit drug detection applications with many absorption features. The other option is to use tunable swept measurements, which would suit gas detection applications where the absorption peaks are of comparable linewidth to the laser. Thermal or electrical tuning and external cavities can provide spectral sweeps, depending on the design of the device in question, allowing for the measurement of both fine and broad features around a specific wavelength. Optical frequency comb (OFC) and SC sources are methods for producing multiple stable wavelengths and are discussed in more detail in Sec. IX.

An advantage of on-chip integration, apart from the benefits for system size and mechanical stability, comes when considering the desirability of wide wavelength tuning of the laser source. Single wavelength lasers with sidemode suppression, such as DFB lasers, have limited tuning. External cavities are required for wider tuning ranges. If the gain material is integrated into a photonic chip, then tuning can be provided by ring resonator systems,[57] providing a compact and tunable source.

On-chip options for laser integration can be divided into the following three main categories, which also apply to hybrid detector integration, notwithstanding the different materials:[58]

- Bonding of fabricated devices, such as by flip-chip bonding, including electrical contacts.
- Bonding of partially fabricated devices or bare epitaxial material, e.g., transfer printing, flip-chip wafers, or tokens/dies.
- Growth or deposition of optical gain material for subsequent fabrication of devices.[59]

All of these approaches are incorporated as backend processes without the need for active alignment, enabling lower cost commercial systems to be manufactured. Within these three broad areas, various coupling mechanisms between the passive waveguide and gain material can be considered:

- Evanescent coupling using tapers for regrowth, wafer bonding, or bonded dies of material.
- Gratings with specific angles for fiber coupling, edge emitting lasers via angle or mirror, or VCSELs.
- End-fire coupling directly to a waveguide facet for either fiber coupling, fiber bonding, or flip-chip bonding of fabricated devices, using a suitable spot size converter such as a taper.

The choice of bonding technique is also critical:

- Wafer bonding, which requires an epitaxial surface and the bonded device structure to be turned face down, will waste a lot of material but give good interface quality.
- Die placement or flip-chipped material will reduce material waste and cost and give a smooth crystal surface at the

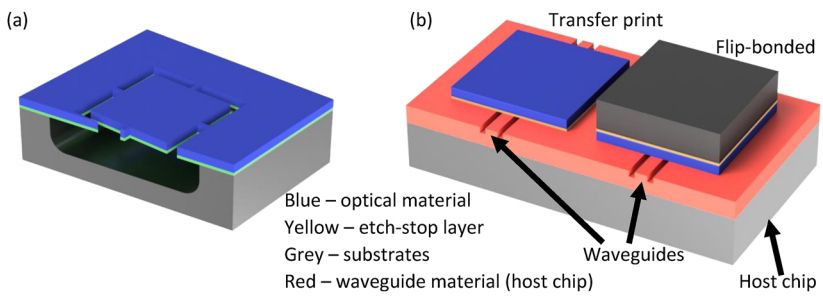

FIG. 4. (a) Cross section of a token prepared for release by wet etching to an etch-stop layer (yellow) and subsequent bonding to a host chip as shown in (b) material placed over tapered waveguides ready for post-processing, left: transfer printed token with the epitaxial surface facing up, and right: a flip-chipped placement (epitaxial surface facing down) of material requiring removal of the substrate (using the etch-stop in yellow).

interface. However, this approach is more complex as the substrate will have to be removed to fabricate devices after bonding, as shown in Fig. 4, and potentially requires etch-stop layers below the active region of the lasers.[60]
- Transfer printing of dies, which are underetched to release material, eliminates the need for post-bonding substrate removal, as shown in Fig. 4. This method also requires etch stop layers to produce these underetched tokens and potentially leaves a rougher interface.

Flip-chip bonding of fully fabricated lasers or detectors enables the testing of these devices, as well as the host chip, before integration. Etched support structures give an exact height alignment, and the bonder aligns in the plane.

It should be noted that mid-IR devices have larger mode sizes and waveguide dimensions compared to those operating at communications bands, i.e., several micrometers as opposed to a few hundred nanometers. This allows for larger mode overlap integrals without the need for spot-size converters when compared to the size of the laser mode.

All these methods have merits for particular applications[61] and all share common challenges in backend processing, cross-contamination, thermal budgets for bonding where dissimilar thermal expansion can cause strain or misalignment, interface quality of coupling devices, and mechanical reliability.

VII. DETECTORS

Waveguide integrated photodetection will be desirable in applications needing a high degree of miniaturization, in more complex systems requiring a large number of photodetectors, or where solid-state integration is wanted for improved environmental robustness. The ideal mid-IR silicon photonic photodetector for sensing would be monolithically integrated with waveguides through a CMOS compatible wafer-scale fabrication process, operate at room temperature, have high responsivity, a low noise equivalent power (NEP), and work at any wavelength across the mid-IR. High bandwidth may not be essential in basic direct absorption spectroscopy systems but would be needed for some more complex low-noise sensing schemes such as wavelength or frequency modulation spectroscopy, dual comb spectroscopy, or heterodyne detection, as well as in free-space communications applications.

Unfortunately, there are no obvious group-IV candidate detector technologies that could be applied throughout the mid-IR. Ge is the most popular material for near-IR photodetection in silicon photonics, but its indirect band edge is at 2 μm, so it becomes a transparent waveguide material rather than a photodetector material at wavelengths beyond this. Its band edge can be extended into the mid-IR by alloying with Sn and introducing strain.[62,63] GeSn photodetectors have been demonstrated at wavelengths up to 4.6 μm in out-of-plane configurations[64] and integrated with SOI waveguides at 2 μm.[65] Due to the limited spectral range, other technologies will be required for fingerprint region applications.

Sub-bandgap states in Si and Ge can lead to defect-mediated absorption, either through intrinsic or extrinsic defects. Room temperature detection up to 2.5 μm is possible in Si PIN diodes in which defects have been created in the Si by ion implantation.[66,67] Excitingly, room temperature subband gap photodetection has also been observed in Ge-on-insulator waveguides at 3.8 μm[68] and in the graded SiGe waveguide platform at 5–10 μm in Refs. 69 and 70. The absorption mechanisms in these works are not yet understood but are thought to be related to defects introduced into the Ge and SiGe crystals, respectively, during their epitaxial growth processes. The wavelength dependence of the Ge absorption mechanism has not yet been explored, whereas the very wide bandwidth of the SiGe absorption is very promising for spectroscopy. The limitations of these devices so far are low responsivities and high dark currents, which may be improved through further device optimization.

As with lasers, the most promising methods for achieving high performance waveguide integrated photodetection across the mid-IR will be through the integration of non-group-IV materials. A monolithic wafer-scale approach would be ideal but is not yet practical. Durlin *et al.* have demonstrated direct epitaxial growth of InAs/InAsSb type-II superlattice (T2SL) detectors on Si substrates[71] with detection up to 6 μm. A GaSb buffer layer was used to solve the problem of lattice mismatch between the Si and T2SL materials. The initial device was illuminated out-of-plane, with further development required for waveguide integration. PbTe detectors have been integrated with chalcogenide waveguides,[72,73] where a polycrystalline PbTe film was deposited directly by thermal evaporation. Since lattice matching is not required, a similar approach could be implemented in group-IV waveguide platforms for detection up to 5 μm.

Heterogeneous integration of more conventional and already optimized mid-IR photodetector materials, e.g., Refs. 74 and 75, would leverage advances in bulk photodetectors. Coupling light out of a waveguide mode into a photodetector can be simpler than coupling light into the waveguide from a laser. For example, an InAsSb photodetector was integrated with an SOI waveguide by bonding a photodetector die on top of a grating coupler, so that the light was coupled from the waveguide into the photodetector material by out-of-plane illumination.[76] A similar approach has not yet been applied to the longer wavelength integration of other detector materials with GOS or SiGe platforms.

The integration of 2D materials with group-IV waveguides offers another route to waveguide integrated mid-IR photodetection, thanks to their broad absorption bandwidths. Graphene can exhibit absorption throughout the mid-IR[77] and has been integrated with mid-IR SOI,[78,79] suspended-Si,[80] and Si-on-CaF_2 waveguides[81] with photodetection shown up to 7.1 μm. The drawbacks of graphene are that it has a zero bandgap, which gives rise to high dark currents, and that it has relatively low absolute absorption, so cavities or plasmonic structures are often used to improve the responsivity. Black phosphorus (BP) on Si waveguide integrated detectors[82,83] has shown better performance, but up to a maximum wavelength of only 4.13 μm.[84] WS_2/HfS_2 (transition metal dichalcogenide) heterostructures are another emerging alternative. Out-of-plane coupled WS_2/HfS_2 photodetectors have shown photodetection with high detectivities up to 10 μm,[85] and a waveguide integrated device has been achieved in the 3.8–5.5 μm range on the silicon-on-sapphire platform.[86] A thorough recent review on the topic of waveguide integrated 2D material-based infrared photodetectors is provided in Ref. 87. The principal drawback to all these devices is that 2D layers on photonic integrated circuit (PIC) platforms are mostly prepared either by mechanical exfoliation or by chemical vapor deposition on a sacrificial substrate followed by a transfer process, with both

methods having low yields and being unsuitable for wafer-scale or high volume-manufacturing.

All of the proposed photoelectric detectors (aside from defect mediated absorption, which is not yet sufficiently well understood in the mid-IR) have some disadvantages relating to the fabrication complexity and scalability, the wavelength range, or the operating temperature. An alternative is to instead consider the integration of thermal photodetectors (i.e., bolometers and pyroelectric detectors) with waveguides, which could be designed to work at any wavelength, work at room temperature, and offer potential for CMOS compatible wafer-scale fabrication. Indeed, bolometers are the most commonly used detection elements in IR sensor arrays. The major drawbacks are worse noise equivalent powers and lower frequency bandwidths. In many sensing applications, the detector frequency may not be relevant if the noise performance is sufficient to meet the required limit of detection.

In 2016, an SOI-based hybrid silicon plasmonic waveguide bolometric photodetector was proposed at 1550 nm[88] with the potential to be extended into the mid-IR. In 2019 and 2021, SOI and suspended-Si waveguide integrated bolometers were demonstrated at 3.8 μm,[89,90] where nanometallic antennas acted as optical absorbers, with the resulting temperature change being measured by monitoring the resistance of an a-Si "thermometer" layer directly below the antennas. The result showed a potential scheme for mid-IR waveguide integration and wafer-scale manufacture, but with relatively low responsivity and NEP.

To achieve higher performance in the future, a thermometer film should be chosen that simultaneously has low electrical resistance (ER) and a high temperature coefficient of resistance. In conventional microbolometers, vanadium oxide is the most popular material (despite the CMOS compatibility issues), followed by amorphous silicon. A TiOx/Ti/TiOx tri-layer film has been optimized for these properties and integrated with waveguide-based bolometers in the 1520–1620 nm range.[91–93] For the responsivity to be further improved, the device geometry should be optimized to reduce thermal conductance while maintaining efficient optical coupling and absorption. Further research could not only improve the bolometer performance by orders of magnitude but also implement similar functionality in the SiGe and GOS platforms for longer wavelength operation. Simulations have been used to show how such devices might be implemented with high responsivities on the GOS platform.[94]

VIII. MODULATORS

Integrated mid-IR modulators may be required for both sensing and free space communications. In bulk absorption spectroscopy systems, modulation is used to improve the signal-to-noise ratio of optical absorption measurements. For example, phase modulators are a key component in frequency modulation spectroscopy systems[95] that can perform extremely high precision absorption measurements.

A. Current state-of-the-art in mid-IR silicon photonics modulators

The simplest method for achieving phase modulation in Si/Ge is to exploit the thermo-optic (TO) effect. A resistive heater is positioned close to a waveguide so that when a current is passed through it, the waveguide is heated locally, and thus, the waveguide's effective refractive index is changed. In the mid-IR, the TO coefficient of Si/Ge reduces slightly compared to its value in the near-IR but nevertheless remains strong. The TO effect is stronger in Ge than in Si: at 3.5 μm wavelength, the TO coefficient of Ge is 2.5 times greater than that of Si.[96] TO modulators have been demonstrated in SOI at 3.8 μm[97] and in GOI at 1.95 μm[98] with a very high efficiency of 7.8 mW/π. To achieve a similar efficiency at longer wavelengths, a suspended Ge-on-SOI platform was used to reduce thermal conduction to the substrate.[99] The key limitation of TO modulators is that their bandwidths are limited by slow thermal diffusion to the 10s of kHz range, which is sufficient for some sensing and switching applications but not for telecommunications.

Where larger bandwidths are required, the free carrier plasma dispersion effect using carrier depletion or carrier injection diodes can be built into waveguides. The free-carrier plasma dispersion effect in the mid-IR in silicon and germanium was investigated by Nedeljkovic *et al.*[100,101] According to those predictions, holes are more absorbing than electrons in Ge, and the change in absorption for both electrons and holes is larger in Ge than in Si for all wavelengths above 3 μm. Therefore, absorption modulators are expected to be more efficient in Ge than in Si at longer wavelengths.

High-speed silicon modulators optimized for the 2 μm band have been demonstrated employing Mach–Zehnder interferometers (MZIs), microring resonators (MRRs), or Michelson interferometers and showed a few tens of Gb/s data rates,[102,103] thus approaching data rates in the near-IR. Currently, the longest wavelength modulators fabricated on SOI substrates are shown operating at the edge of the SiO2 transparency range at 3.8 μm.[104] PIN diodes were used as phase shifters to inject carriers in an MZI by using the free-carrier electrorefraction effect and in a variable optical attenuator (VOA) by using the free-carrier electroabsorption effect. The cross section of the diode used in both configurations is shown in Fig. 5. The data rates were up to 125 Mbit/s,[104] which is not surprising since optical mode size scales with wavelength and Ohmic contacts need to be placed further away, thus increasing the volume of the intrinsic region of the device as well as diode junction resistance, which limits modulation efficiency and bandwidth.

Ge-on-Si injection modulators have been demonstrated to operate at 3.8 and 8 μm.[104] They were based on PIN diodes integrated with Ge rib waveguides with a 3 μm core thickness. Two different types of modulators were demonstrated on this platform: VOAs and MZIs. GOS modulators with lengths of 1–2 mm showed ER up to 35 dB and data rates up to 60 Mbit/s.[104] Measurements showed that the injected carrier absorption coefficient was 4.9 times

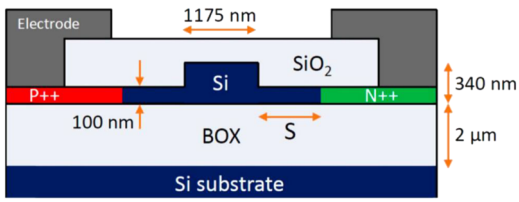

FIG. 5. Schematic cross section of SOI injection modulators, reproduced with permission from Nedeljkovic *et al.*, Opt. Lett. **44**(4), 915–918 (2019). Copyright 2019 Author(s), licensed under a Creative Commons Attribution 4.0 License.

greater at 8 μm compared to 3.8 μm at the same injection current (per unit length), which was close to the prediction from Ref. 101. Extremely broadband graded index SiGe modulators have reached 1.5 GHz modulation across the 5.5–10 μm wavelength range by integrating a vertical PIN diode into the structure.[70] The major problem with these modulators was that they could not achieve low insertion loss and a high extinction ratio at the same time, and further optimization will be needed to improve their performance.

B. Prospects for mid-IR silicon photonics modulators

The performance of mid-IR optical modulators on Si- and Ge-based platforms has shown significant progress over the last few years. However, there is still a lot of room for improvement. Modulators in the 2 μm band will need to be optimized to reach data rates close to very recent results in the near-IR and integrated with electronics to reduce power consumption. Modulators at longer wavelengths need to be redesigned to achieve lower insertion losses and larger extinction ratios, so they are unlikely to be included in early mid-IR sensor circuits. In addition, heterogeneous configurations need to be explored more extensively, and materials with larger modulation effects (e.g., LiNbO3 and BaTiO3) can be integrated with Si and Ge. In any case, modulators can play a significant role in improving future mid-IR sensing and communications systems.

IX. NONLINEAR MID-IR PHOTONICS

A. Current state-of-the-art in nonlinear mid-IR photonics

An alternative to the laser sources discussed in Sec. VIII is to exploit the nonlinearity of the silicon materials to generate multiple wavelengths of light for the applications of interest. The dominant nonlinearity in silicon is the third order susceptibility that gives rise to processes such as self-phase modulation, four-wave mixing (FWM), and Raman scattering,[105] which can be used for the generation of new wavelengths when pumped with high light intensities. Such sources can be designed for broadband light generation or discrete tunable systems and are best used when spectral bandwidth is the priority rather than the absolute source intensity. This means nonlinear sources are particularly suitable for applications such as drug detection, where multiple stable mid-IR wavelengths are required to identify the analyte and quantify its concentration.

Compared with conventional nonlinear platforms such as highly nonlinear fibers (HNLF) and $\chi^{(2)}$ materials that meet challenges when integrated with photonics platforms, SOI platforms possess distinct advantages in integration due to the mature CMOS technology. Advanced manufacturing techniques ensure precise structural control, enabling efficient adjustment of dispersion profiles through waveguide dispersion.[106] The design of wavelength-scale structures also enables the achievement of a small effective mode area and footprint to minimize the device size. In addition, the high refractive index contrast between the cladding and core materials results in tight light confinement. This leads to high light intensities in the waveguide cores, which is a crucial factor for the observation of nonlinear effects.

The typical integrated materials, such as Si, Ge, and SiN, have large Kerr parameters and relatively strong Raman gains, when compared to glass fibers, which dominate nonlinear performance. The nonlinear performance of Si in the telecom band has been extensively explored.[107–111] However, the efficiency is limited by two-photon absorption (TPA) and its induced free carrier absorption (FCA). The traditional method to alleviate FCA is to use a p-i-n diode operating under reverse bias,[108] although the influence of TPA still persists. Shifting the operating wavelength to the mid-IR band shows promise in eliminating TPA in Si, especially as it becomes negligible for wavelengths >2.2 μm. Four-wave mixing (FWM) is a useful nonlinear process that can be used to construct tunable light sources and amplifiers that has been successfully demonstrated in the mid-IR band using SOI waveguides.[112–114] Thanks to the low nonlinear losses, relatively high conversion efficiencies of up to ~−18 dB can be obtained, with bandwidths exceeding 700 nm. However, as typical linear losses for the SOI waveguides in the mid-IR band are above 1 dB/cm, alternative materials such as SiN, which exhibits an extremely low loss of 0.1 dB/cm at 3 μm,[115] have also been explored. A tunable FWM source covering the wavelength range of 2.6–3.6 μm was demonstrated using different waveguides on the same chip, although with reduced conversion efficiencies of ~−30 dB due to the lower nonlinear coefficient of the SiN material.

Apart from FWM, Raman scattering is another important nonlinear effect that can be used for developing on-chip light sources. In contrast to other Raman materials, silicon has a wide transparency window of up to 8 μm and a high damage threshold so that it can support high power operation.[116] Although Raman amplification has been reported at 2.2 μm in a silicon core fiber (up to 30 dB peak gain)[117] and at 3.39 μm in a bulk silicon crystal (with ~12 dB gain),[118] mid-IR amplification has yet to be experimentally demonstrated on an integrated Si platform. However, the feasibility of on-chip Raman lasers has been theoretically validated,[119–121] showing the potential for the production of cascaded Raman systems that could operate out to 3–5 μm. Possible limitations for mid-IR Raman light sources include three photon absorption (3PA) and its induced FCA due to the high light intensity needed for strong Raman scattering.[122] Moreover, as the Raman gain is inversely proportional to wavelength, the Raman effect weakens in the mid-IR compared to that in the telecom band, thus requiring even higher pump powers.

In addition to sources, spectroscopy systems have also been successfully developed through the use of optical frequency combs (OFCs) and supercontinuum generation (SCG).[123,124] Although SOI and SiN waveguides have been used to achieve OFCs and SCG from 1.5 to 3.5 μm, extending the bandwidth to longer wavelengths is limited by the significant cladding absorption above 4 μm.[125–129] To overcome material absorption, air claddings have proven effective for fully exploiting the transparency window of silicon, while Ge or Ge-rich SiGe core materials can be used to extend the upper wavelength limit of the generated light. For example, OFC and SCG generated by suspended silicon waveguides have been demonstrated up to 8.8 μm,[123] and the long wavelength edge has been extended out to 12 μm by using suspended Ge waveguides.[130–132] Furthermore, a recent demonstration of on-chip GaAs waveguides shows SCG extending over a wavelength range covering 4–9 μm,[133] indicating progress in developing new integrated materials for nonlinear applications.

B. Prospects for nonlinear mid-IR photonics

Reflecting on the use of Si and Ge platforms for nonlinear applications, there has been considerable success in the development of systems based around FWM, SCG, and OFC. Although the translation of Raman gain from the telecom band to the mid-IR band has encountered a persistent bottleneck, theoretical work has shown that overcoming this would be valuable for applications requiring high power and tunability sources. Thus, achieving experimental breakthroughs in this area necessitates further concerted efforts. However, the relatively low output powers of the current nonlinear systems pose an additional constraint on the practical implementation of these devices, which needs to be addressed through waveguide design and loss reduction. Finally, the current utilization of free space coupling for on-chip nonlinear devices emphasizes the need to explore integration strategies for realizing fully functional devices in the mid-IR band, thereby enabling their widespread commercial applications.

X. PERSPECTIVES AND CHALLENGES OF INTEGRATION

The mechanisms by which lasers and detectors are integrated into a sensing system have performance, cost, and complexity implications. For silicon photonics, integration broadly falls into two categories: on-chip or off-chip. Both have challenges and limitations affecting system design.

The purpose of a photonic sensor is a key question for its integration and needs to be considered at an early stage. For example, the requirements of a disposable home-based medical test are different from those required at a local clinic. Both may need to give results more rapidly than a hospital, preferably within the timescale of a consultation, but not necessarily as accurately as those at a hospital, i.e., as an early screening tool. In a hospital environment, the timescales may be different depending on the nature of the application. For example, drug detection measurements may need to provide rapid data for urgent and critical treatment of a patient, whereas cancer diagnosis will need to be more accurate but with less critical timescales.

Large and expensive high-power lasers may be incorporated off-chip if the environment has the required space and if the system does not need to be portable or low cost. This is not the case for a mass-produced portable system in a clinic where the integration of sources and detectors needs to be cheaper and more compact. In this case, a system with a disposable component will often be required to eliminate cross-contamination. However, reducing waste is ecologically important. Even if the mass production of mid-IR lasers were to reduce the cost to a point where a disposable system might include the laser, this would not be desirable in terms of environmental impact.

Incorporating a disposable sensing chip that does not include expensive and potentially reusable components necessitates either completely off-chip systems for sources and detectors or a hybrid on- and off-chip design where lasers and detectors are integrated onto silicon photonics chips and coupled to a disposable transducer chip. Coupling could be achieved by gratings, end-fire couplers with spot size converters, or evanescent coupling via tapers on either component. Evanescent coupling is a technique recently demonstrated with large alignment tolerances at communications wavelengths.[134]

The ideal scenario for inter-chip coupling is for untrained users to be able to quickly and easily use the device. Active alignment could be used as a solution for final micropositioning. Without the need for permanent bonding of the components for this theoretical disposable system, this becomes a viable option and can either be achieved manually, guided by simple indicators such as an LED array, or automatically, akin to the autofocus of a camera.

Environmental monitoring applications may necessitate a fully integrated system because typical operating scenarios (e.g., in a remote location or on an autonomous submarine 6 km below sea level) often do not allow user access, or fully independent remote operation may be desirable to keep operational and maintenance costs low. In such cases, the environment in which the device will be used is another critical issue to address. The need for robust systems available to withstand high pressure, mechanical impact, and vibration is critical. Such systems may need to be pressure and vibration tested for mechanical strength and electrical operation. In this case, on-chip integration of the detectors and sources becomes very attractive as the components can be potted with suitable materials, eliminating the need for protection of delicate optical interconnects. Potting compounds may be used to enhance the overall strength of bonded devices, eliminate vibrational movement between components, and reduce thermal expansion differences by pinning components but inducing strain. These effects need to be considered along with the effects of such potting compounds on the performance and coupling of the lasers or detectors.

The choice of bonding techniques will also be important when considering multiple devices, as in a fully integrated system with both lasers and detectors on chip. Thermal budgets and localized heating will need to be considered. For example, will a solder or polymer reflow during the bonding of subsequent devices? Possible approaches to counteract this might be to use bonding media with different reflow temperatures, localized heating of the bond (e.g., laser spot absorbed by the substrate), one die of material utilizing a gain medium as a laser in one section and an absorber in another, or multiple dies placed at the same time using a host carrier wafer (producing an extra source of potential misalignment).

XI. CONCLUSION

Significant progress has been made toward achieving integrated mid-IR silicon photonics sensors. There are several areas that require significant work if suitable systems-level integration is to be achieved, which we argue will be necessary for scientific and commercial exploitation. Mid-IR applications are clearly defined, especially in the healthcare and environmental monitoring sectors, and have been validated using bench-top equipment. This has largely been done using FTIR spectrometers, but there have also been many demonstrations of ICLs used for the detection of methane and other gases.

Research in components and devices shows strong recent progress. Waveguide losses, coupling efficiencies, and modulator bandwidths show decent performance, although not to the level of near-IR components and devices that operate at telecommunications wavelengths, but still good enough to warrant integration. Robust and repeatable inter-chip coupling strategies are the obvious shortcoming. We have shown how it is not desirable to have

full on-chip integration for healthcare applications, for example, but these require simple coupling systems that can be operated by the non-expert user if mid-IR silicon photonics PICs are to achieve widespread adoption. Partial integration has been shown, e.g., QCLs directly coupled to waveguides or microfluidics with photonics transducers. We have also discussed how the nonlinearity of the materials can significantly expand the functionality of mid-IR platforms, but the propagation loss is not yet low enough to fully exploit this technology. This means the integration of nonlinear mid-IR devices is a second area requiring significant effort.

Work should now focus on completing integration for a specific application. This need not have everything on a single chip; the applications requiring single chip integration are likely to have more challenging robustness requirements for deep oceans or space. This emphasizes the need for a holistic application-driven system-level approach with robust inter-chip coupling. Mid-IR sensing has a crucial advantage over other low-cost sensors because the method itself provides analyte specificity. It does not require surface functionalization or binding, so mid-IR sensing chips do not have an expiration date or require storage in a freezer. With appropriate engineering for the non-expert user, mid-IR sensors could become ubiquitous.

SUPPLEMENTARY MATERIAL

In the supplementary material, Table I provides the numeric data used to plot the graph shown in Fig. 3, together with the references from which the data are taken.

ACKNOWLEDGMENTS

The authors gratefully acknowledge the funding from the Engineering and Physical Sciences Research Council (Grant Nos. EP/V047663/1, EP/W035995/1, and EP/N00762X/1) and the Royal Academy of Engineering (Grant No. RF201617/16/33).

AUTHOR DECLARATIONS

Conflict of Interest

The authors have no conflicts to disclose.

Author Contributions

Colin J. Mitchell: Writing – original draft (equal); Writing – review & editing (equal). **Tianhui Hu**: Writing – original draft (equal); Writing – review & editing (equal). **Shiyu Sun**: Writing – original draft (equal); Writing – review & editing (equal). **Callum J. Stirling**: Visualization (supporting); Writing – original draft (equal); Writing – review & editing (equal). **Milos Nedeljkovic**: Supervision (equal); Writing – original draft (equal); Writing – review & editing (equal). **Anna C. Peacock**: Supervision (equal); Writing – original draft (equal); Writing – review & editing (equal). **Graham T Reed**: Funding acquisition (equal); Supervision (equal); Writing – review & editing (equal). **Goran Z. Mashanovich** Conceptualization (equal); Funding acquisition (equal); Supervision (equal); Writing – original draft (equal); Writing – review & editing (equal). **David J. Rowe** Visualization (lead); Writing – original draft (lead); Writing – review & editing (lead).

DATA AVAILABILITY

The data that support the findings of this study are available within the article and its supplementary material.

REFERENCES

[1]L. Tombez, E. J. Zhang, J. S. Orcutt, S. Kamlapurkar, and W. M. J. Green, "Methane absorption spectroscopy on a silicon photonic chip," Optica **4**(11), 1322–1325 (2017).
[2]M. Vlk, A. Datta, S. Alberti, H. D. Yallew *et al.*, "Extraordinary evanescent field confinement waveguide sensor for mid-infrared trace gas spectroscopy," Light: Sci. Appl. **10**(1), 26 (2021).
[3]H. D. Yallew, M. Vlk, A. Datta, S. Alberti *et al.*, "Sub-ppm methane detection with mid-infrared slot waveguides," ACS Photonics **10**(12), 4282–4289 (2023).
[4]W. Liu, Y. Ma, X. Liu, J. Zhou *et al.*, "Larger-than-unity external optical field confinement enabled by metamaterial-assisted comb waveguide for ultrasensitive long-wave infrared gas spectroscopy," Nano Lett. **22**(15), 6112–6120 (2022).
[5]Y.-C. Chang, P. Wägli, V. Paeder, A. Homsy *et al.*, "Cocaine detection by a mid-infrared waveguide integrated with a microfluidic chip," Lab Chip **12**(17), 3020–3023 (2012).
[6]P. Wägli, Y. C. Chang, A. Homsy, L. Hvozdara *et al.*, "Microfluidic droplet-based liquid-liquid extraction and on-chip IR spectroscopy detection of cocaine in human saliva," Anal. Chem. **85**(15), 7558–7565 (2013).
[7]V. Mittal, G. Devitt, M. Nedeljkovic, L. G. Carpenter *et al.*, "Ge on Si waveguide mid-infrared absorption spectroscopy of proteins and their aggregates," Biomed. Opt. Express **11**(8), 4714–4722 (2020).
[8]V. Mittal, M. Nedeljkovic, L. G. Carpenter, A. Z. Khokhar *et al.*, "Waveguide absorption spectroscopy of bovine serum albumin in the mid-infrared fingerprint region," ACS Sens. **4**(7), 1749–1753 (2019).
[9]H. J. Butler, P. M. Brennan, J. M. Cameron, D. Finlayson *et al.*, "Development of high-throughput ATR-FTIR technology for rapid triage of brain cancer," Nat. Commun. **10**(1), 4501 (2019).
[10]A. Sala, J. M. Cameron, C. A. Jenkins, H. Barr *et al.*, "Liquid biopsy for pancreatic cancer detection using infrared spectroscopy," Cancers **14**(13), 3048 (2022).
[11]M. Huber, K. V. Kepesidis, L. Voronina, F. Fleischmann *et al.*, "Infrared molecular fingerprinting of blood-based liquid biopsies for the detection of cancer," eLife **10**, e68758 (2021).
[12]V. G. Barauna, M. N. Singh, L. L. Barbosa, W. D. Marcarini *et al.*, "Ultrarapid on-site detection of SARS-CoV-2 infection using simple ATR-FTIR spectroscopy and an analysis algorithm: High sensitivity and specificity," Anal. Chem. **93**(5), 2950–2958 (2021).
[13]E. P. Mwanga, E. G. Minja, E. Mrimi, M. G. Jiménez *et al.*, "Detection of malaria parasites in dried human blood spots using mid-infrared spectroscopy and logistic regression analysis," Malar. J. **18**(1), 341 (2019).
[14]J. Fedeli and S. Nicoletti, "Mid-infrared (Mid-IR) silicon-based photonics," Proc. IEEE **106**(12), 2302–2312 (2018).
[15]G. Z. Mashanovich, M. Nedeljkovic, J. Soler-Penades, Z. Qu *et al.*, "Group IV mid-infrared photonics [Invited]," Opt. Mater. Express **8**(8), 2276–2286 (2018).
[16]M. S. Rouifed, C. G. Littlejohns, G. X. Tina, Q. Haodong *et al.*, "Low loss SOI waveguides and MMIs at the MIR wavelength of 2 μm," IEEE Photonics Technol. Lett. **28**(24), 2827–2829 (2016).
[17]N. Hattasan, B. Kuyken, F. Leo, E. M. P. Ryckeboer *et al.*, "High-efficiency SOI fiber-to-chip grating couplers and low-loss waveguides for the short-wave infrared," IEEE Photonics Technol. Lett. **24**(17), 1536–1538 (2012).
[18]G. Z. Mashanovich, M. M. Miloševic, M. Nedeljkovic, N. Owens *et al.*, "Low loss silicon waveguides for the mid-infrared," Opt. Express **19**(8), 7112–7119 (2011).
[19]M. Nedeljkovic, A. Z. Khokhar, Y. Hu, X. Chen *et al.*, "Silicon photonic devices and platforms for the mid-infrared," Opt. Mater. Express **3**(9), 1205–1214 (2013).
[20]P. T. Lin, V. Singh, Y. Cai, L. C. Kimerling, and A. Agarwal, "Air-clad silicon pedestal structures for broadband mid-infrared microphotonics," Opt. Lett. **38**(7), 1031–1033 (2013).

[21]C. J. Stirling, W. Cao, J. D. Reynolds, Z. Qu *et al.*, "Mid-infrared silicon-on-insulator waveguides with single-mode propagation over an octave of frequency," Opt. Express **30**(6), 8560–8570 (2022).
[22]J. S. Penadés, A. Z. Khokhar, M. Nedeljkovic, and G. Z. Mashanovich, "Low-loss mid-infrared SOI slot waveguides," IEEE Photonics Technol. Lett. **27**(11), 1197–1199 (2015).
[23]F. Li, S. D. Jackson, C. Grillet, E. Magi *et al.*, "Low propagation loss silicon-on-sapphire waveguides for the mid-infrared," Opt. Express **19**(16), 15212–15220 (2011).
[24]T. Baehr-Jones, A. Spott, R. Ilic, A. Spott *et al.*, "Silicon-on-sapphire integrated waveguides for the mid-infrared," Opt. Express **18**(12), 12127–12135 (2010).
[25]S. Khan, J. Chiles, J. Ma, and S. Fathpour, "Silicon-on-nitride waveguides for mid- and near-infrared integrated photonics," Appl. Phys. Lett. **102**(12), 121104 (2013).
[26]W. Zhou, Z. Cheng, X. Wu, X. Sun, and H. K. Tsang, "Fully suspended slot waveguide platform," J. Appl. Phys. **123**(6), 063103 (2018).
[27]Z. Cheng, X. Chen, C. Y. Wong, K. Xu, and H. K. Tsang, "Mid-infrared suspended membrane waveguide and ring resonator on silicon-on-insulator," IEEE Photonics J. **4**(5), 1510–1519 (2012).
[28]J. S. Penades, A. Ortega-Moñux, M. Nedeljkovic, J. G. Wangüemert-Pérez *et al.*, "Suspended silicon mid-infrared waveguide devices with subwavelength grating metamaterial cladding," Opt. Express **24**(20), 22908–22916 (2016/10/2016).
[29]W. Liu, Y. Ma, Y. Chang, B. Dong *et al.*, "Suspended silicon waveguide platform with subwavelength grating metamaterial cladding for long-wave infrared sensing applications," Nanophotonics **10**(7), 1861–1870 (2021).
[30]J. S. Penadés, A. Sánchez-Postigo, M. Nedeljkovic, A. Ortega-Moñux *et al.*, "Suspended silicon waveguides for long-wave infrared wavelengths," Opt. Lett. **43**(4), 795–798 (2018).
[31]M. Nedeljkovic, J. S. Penadés, C. J. Mitchell, A. Z. Khokhar *et al.*, "Surface-grating-coupled low-loss Ge-on-Si rib waveguides and multimode interferometers," IEEE Photonics Technol. Lett. **27**(10), 1040–1043 (2015).
[32]Y.-C. Chang, V. Paeder, L. Hvozdara, J.-M. Hartmann, and H. P. Herzig, "Low-loss germanium strip waveguides on silicon for the mid-infrared," Opt. Lett. **37**(14), 2883–2885 (2012).
[33]M. Nedeljkovic, J. S. Penades, V. Mittal, G. S. Murugan *et al.*, "Germanium-on-silicon waveguides operating at mid-infrared wavelengths up to 85 μm," Opt. Express **25**(22), 27431–27441 (2017).
[34]K. Gallacher, R. W. Millar, U. Griškevičiūte, L. Baldassarre *et al.*, "Low loss Ge-on-Si waveguides operating in the 8–14 μm atmospheric transmission window," Opt. Express **26**(20), 25667–25675 (2018).
[35]D. A. Kozak, T. H. Stievater, R. Mahon, and W. S. Rabinovich, "Germanium-on-silicon waveguides at wavelengths from 6.85 to 11.25 microns," IEEE J. Sel. Top. Quantum Electron. **24**(6), 1–4 (2018).
[36]J. Lim, J. Shim, D. M. Geum, and S. Kim, "Experimental demonstration of germanium-on-silicon slot waveguides at mid-infrared wavelength," IEEE Photonics J. **14**(3), 1–9 (2022).
[37]D. A. Kozak, N. F. Tyndall, M. W. Pruessner, W. S. Rabinovich, and T. H. Stievater, "Germanium-on-silicon waveguides for long-wave integrated photonics: Ring resonance and thermo-optics," Opt. Express **29**(10), 15443–15451 (2021).
[38]W. Li, P. Anantha, S. Bao, K. H. Lee *et al.*, "Germanium-on-silicon nitride waveguides for mid-infrared integrated photonics," Appl. Phys. Lett. **109**(24), 241101 (2016).
[39]T.-H. Xiao, Z. Zhao, W. Zhou, C.-Y. Chang *et al.*, "Mid-infrared high-*Q* germanium microring resonator," Opt. Lett. **43**(12), 2885–2888 (2018).
[40]A. Osman, M. Nedeljkovic, J. Soler Penades, Y. Wu *et al.*, "Suspended low-loss germanium waveguides for the longwave infrared," Opt. Lett. **43**(24), 5997–6000 (2018).
[41]A. Sánchez-Postigo, A. Ortega-Moñux, J. Soler Penadés, A. Osman *et al.*, "Suspended germanium waveguides with subwavelength-grating metamaterial cladding for the mid-infrared band," Opt. Express **29**(11), 16867–16878 (2021).
[42]P. T. Lin, V. Singh, H.-Y. G. Lin, T. Tiwald *et al.*, "Low-stress silicon nitride platform for mid-infrared broadband and monolithically integrated microphotonics," Adv. Opt. Mater. **1**(10), 732–739 (2013).
[43]P. Tai Lin, V. Singh, L. Kimerling, and A. Murthy Agarwal, "Planar silicon nitride mid-infrared devices," Appl. Phys. Lett. **102**(25), 251121 (2013).
[44]J. Zhou, D. Al Husseini, J. Li, Z. Lin *et al.*, "Detection of volatile organic compounds using mid-infrared silicon nitride waveguide sensors," Sci. Rep. **12**(1), 5572 (2022).
[45]M. Sinobad, A. DellaTorre, R. Armand, B. Luther-Davies *et al.*, "Mid-infrared supercontinuum generation in silicon-germanium all-normal dispersion waveguides," Opt. Lett. **45**(18), 5008–5011 (2020).
[46]M. Brun, P. Labeye, G. Grand, J.-M. Hartmann *et al.*, "Low loss SiGe graded index waveguides for mid-IR applications," Opt. Express **22**(1), 508–518 (2014).
[47]J. M. Ramirez, Q. Liu, V. Vakarin, J. Frigerio *et al.*, "Graded SiGe waveguides with broadband low-loss propagation in the mid infrared," Opt. Express **26**(2), 870–877 (2018).
[48]M. Montesinos-Ballester, V. Vakarin, Q. Liu, X. Le Roux *et al.*, "Ge-rich graded SiGe waveguides and interferometers from 5 to 11 μm wavelength range," Opt. Express **28**(9), 12771–12779 (2020).
[49]Q. Liu, J. M. Ramirez, V. Vakarin, X. Le Roux *et al.*, "Mid-infrared sensing between 52 and 66 μm wavelengths using Ge-rich SiGe waveguides [Invited]," Opt. Mater. Express **8**(5), 1305–1312 (2018).
[50]T. Peng and Z. You, "Reliability of MEMS in shock environments: 2000–2020," Micromachines **12**(11), 1275 (2021).
[51]N. T. Benéitez, B. Baumgartner, J. Missinne, S. Radosavljevic *et al.*, "Mid-IR sensing platform for trace analysis in aqueous solutions based on a germanium-on-silicon waveguide chip with a mesoporous silica coating for analyte enrichment," Opt. Express **28**(18), 27013–27027 (2020).
[52]R. F. Kazarinov and R. A. Suris, "Possibility of the amplification of electromagnetic waves in a semiconductor with a superlattice," Sov. Phys. - Semicond. **5**(4), 707–709 (1971).
[53]J. Faist, F. Capasso, D. L. Sivco, C. Sirtori *et al.*, "Quantum cascade laser," Science **264**(5158), 553–556 (1994).
[54]R. Q. Yang, "Infrared laser based on intersubband transitions in quantum wells," Superlattices Microstruct. **17**(1), 77–83 (1995).
[55]S. Slivken, D. Wu, and M. Razeghi, "Surface emitting, tunable, mid-infrared laser with high output power and stable output beam," Sci. Rep. **9**(1), 549 (2019).
[56]N. Li, G. Chen, D. K. T. Ng, L. W. Lim *et al.*, "Integrated lasers on silicon at communication wavelength: A progress review," Adv. Opt. Mater. **10**(23), 2201008 (2022).
[57]T. Komljenovic, L. Liang, R. L. Chao, J. Hulme *et al.*, "Widely-tunable ring-resonator semiconductor lasers," Appl. Sci. **7**(7), 732 (2017).
[58]M. Piels and J. E. Bowers, "Photodetectors for silicon photonic integrated circuits," in *Photodetectors: Materials, Devices and Applications* (Woodhead Publishing, 2016), pp. 3–20.
[59]A. Remis, L. Monge-Bartolome, M. Paparella, A. Gilbert *et al.*, "Unlocking the monolithic integration scenario: Optical coupling between GaSb diode lasers epitaxially grown on patterned Si substrates and passive SiN waveguides," Light: Sci. Appl. **12**(1), 150 (2023).
[60]A. Spott, E. J. Stanton, A. Torres, M. L. Davenport *et al.*, "Interband cascade laser on silicon," Optica **5**(8), 996–1005 (2018).
[61]M. Tang, J. S. Park, Z. Wang, S. Chen *et al.*, "Integration of III-V lasers on Si for Si photonics," Prog. Quantum Electron. **66**, 1–18 (2019).
[62]A. Gassenq, F. Gencarelli, J. Van Campenhout, Y. Shimura *et al.*, "GeSn/Ge heterostructure short-wave infrared photodetectors on silicon," Opt. Express **20**(25), 27297–27303 (2012).
[63]H. Tran, T. Pham, J. Margetis, Y. Zhou *et al.*, "Si-based GeSn photodetectors toward mid-infrared imaging applications," ACS Photonics **6**(11), 2807–2815 (2019).
[64]M. R. M. Atalla, S. Assali, A. Attiaoui, C. Lemieux-Leduc *et al.*, "All-group IV transferable membrane mid-infrared photodetectors," Adv. Funct. Mater. **31**(3), 2006329 (2021).
[65]J. Wang, X. Wang, Y. Li, Y. Yang *et al.*, "High-responsivity on-chip waveguide coupled germanium photodetector for 2 μm waveband," Photonics Res. **12**(1), 115–122 (2024).
[66]D. J. Thomson, L. Shen, J. J. Ackert, E. Huante-Ceron *et al.*, "Optical detection and modulation at 2μm-25μm in silicon," Opt. Express **22**(9), 10825–10830 (2014).
[67]J. J. Ackert, D. J. Thomson, L. Shen, A. C. Peacock *et al.*, "High-speed detection at two micrometres with monolithic silicon photodiodes," Nat. Photonics **9**(6), 393–396 (2015).

[68]L. Reid, M. Nedeljkovic, W. Cao, L. Mastronardi *et al.*, "Photodetection at 3.8 μm using intrinsic monolithic integrated germanium photodiodes," in *2021 IEEE 17th International Conference on Group IV Photonics* (IEEE, 2021), pp. 1–2.
[69]T. H. N. Nguyen, N. Koompai, V. Turpaud, M. Montesinos-Ballester *et al.*, "Room temperature-integrated photodetector between 5 μm and 8 μm wavelength," Adv. Photonics Res. **4**(2), 2200237 (2023).
[70]T. H. N. Nguyen, V. Turpaud, N. Koompai, J. Peltier *et al.*, "Integrated pin modulator and photodetector operating in the mid-infrared range from 5.5 μm to 10 μm," Nanophotonics **13**(10), 1803–1813 (2024).
[71]Q. Durlin, J. P. Perez, L. Cerutti, J. B. Rodriguez *et al.*, "Midwave infrared barrier detector based on Ga-free InAs/InAsSb type-II superlattice grown by molecular beam epitaxy on Si substrate," Infrared Phys. Technol. **96**, 39–43 (2019).
[72]Z. Han, V. Singh, D. Kita, C. Monmeyran *et al.*, "On-chip chalcogenide glass waveguide-integrated mid-infrared PbTe detectors," Appl. Phys. Lett. **109**(7), 071111 (2016).
[73]P. Su, Z. Han, D. Kita, P. Becla *et al.*, "Monolithic on-chip mid-IR methane gas sensor with waveguide-integrated detector," Appl. Phys. Lett. **114**(5), 051103 (2019).
[74]P. Martyniuk and A. Rogalski, "Hot infrared photodetectors," Opto-Electron. Rev. **21**(2), 239–257 (2013).
[75]P. Martyniuk, A. Rogalski, and S. Krishna, "Interband quantum cascade infrared photodetectors: Current status and future trends," Phys. Rev. Appl. **17**(2), 027001 (2022).
[76]M. Muneeb, X. Chen, P. Verheyen, G. Lepage *et al.*, "Demonstration of silicon-on-insulator mid-infrared spectrometers operating at 38 μm," Opt. Express **21**(10), 11659–11669 (2013).
[77]S. Yuan, R. Yu, C. Ma, B. Deng *et al.*, "Room temperature graphene mid-infrared bolometer with a broad operational wavelength range," ACS Photonics **7**(5), 1206–1215 (2020).
[78]J. Guo, J. Li, C. Liu, Y. Yin *et al.*, "High-performance silicon–graphene hybrid plasmonic waveguide photodetectors beyond 1.55 μm," Light: Sci. Appl. **9**(1), 29 (2020).
[79]Z. Qu, M. Nedeljkovic, Y. Wu, J. Soler Penades *et al.*, "Waveguide integrated graphene mid-infrared photodetector," Proc. SPIE **10537**, 105371N (2018).
[80]X. Wang, Z. Cheng, K. Xu, H. K. Tsang, and J. B. Xu, "High-responsivity graphene/silicon-heterostructure waveguide photodetectors," Nat. Photonics **7**(11), 888–891 (2013).
[81]Y. Ma, Y. Chang, B. Dong, J. Wei *et al.*, "Heterogeneously integrated graphene/silicon/halide waveguide photodetectors toward chip-scale zero-bias long-wave infrared spectroscopic sensing," ACS Nano **15**(6), 10084–10094 (2021).
[82]Y. Ma, B. Dong, J. Wei, Y. Chang *et al.*, "High-responsivity mid-infrared black phosphorus slow light waveguide photodetector," Adv. Opt. Mater. **8**(13), 2000337 (2020).
[83]Y. Yin, R. Cao, J. Guo, C. Liu *et al.*, "High-speed and high-responsivity hybrid silicon/black-phosphorus waveguide photodetectors at 2 μm," Laser Photonics Rev. **13**(6), 1900032 (2019).
[84]P. L. Chen, Y. Chen, T. Y. Chang, W. Q. Li *et al.*, "Waveguide-integrated van der Waals heterostructure mid-infrared photodetector with high performance," ACS Appl. Mater. Interfaces **14**(21), 24856–24863 (2022).
[85]S. Lukman, L. Ding, L. Xu, Y. Tao *et al.*, "High oscillator strength interlayer excitons in two-dimensional heterostructures for mid-infrared photodetection," Nat. Nanotechnol. **15**(8), 675–682 (2020).
[86]S. Edelstein, S. R. K. C. Indukuri, N. Mazurski, and U. Levy, "Waveguide-integrated mid-IR photodetector and all-optical modulator based on interlayer excitons absorption in a WS_2/HfS_2 heterostructure," Nanophotonics **11**(19), 4337–4345 (2022).
[87]G. Y. Huang, Y. Hao, S. Q. Li, Y. D. Jia *et al.*, "Recent progress in waveguide-integrated photodetectors based on 2D materials for infrared detection," J. Phys. D: Appl. Phys. **56**(11), 113001 (2023).
[88]H. Wu, K. Ma, Y. Shi, L. Wosinski, and D. Dai, "Ultracompact on-chip photothermal power monitor based on silicon hybrid plasmonic waveguides," Nanophotonics **6**(5), 1121–1131 (2017).
[89]Y. Wu, Z. Qu, A. Osman, W. Cao *et al.*, "Mid-infrared nanometallic antenna assisted silicon waveguide based bolometers," ACS Photonics **6**(12), 3253–3260 (2019).
[90]Y. Wu, Z. Qu, A. Osman, C. Wei *et al.*, "Nanometallic antenna-assisted amorphous silicon waveguide integrated bolometer for mid-infrared," Opt. Lett. **46**(3), 677–680 (2021).
[91]J. Shim, J. Lim, D. M. Geum, B. H. Kim *et al.*, "Tailoring bolometric properties of a $TiO_x/Ti/TiO_x$ tri-layer film for integrated optical gas sensors," Opt. Express **29**(12), 18037–18058 (2021).
[92]J. Shim, J. Lim, D. M. Geum, J. B. You *et al.*, "High-sensitivity waveguide-integrated bolometer based on free-carrier absorption for Si photonic sensors," Opt. Express **30**(23), 42663–42677 (2022).
[93]J. Shim, J. Lim, D. M. Geum, J. B. You *et al.*, "TiOx/Ti/TiOx tri-layer film-based waveguide bolometric detector for on-chip Si photonic sensor," IEEE Trans. Electron Devices **69**(4), 2151–2158 (2022).
[94]X. Liu, R. Ma, J. Liu, S. Zheng *et al.*, "Metasurface-assisted amorphous germanium-tin waveguide bolometer for mid-infrared photodetection," Opt. Express **32**(3), 3501–3511 (2024).
[95]G. C. Bjorklund, "Frequency-modulation spectroscopy: A new method for measuring weak absorptions and dispersions," Opt. Lett. **5**(1), 15–17 (1980).
[96]B. J. Frey, D. B. Leviton, and T. J. Madison, "Temperature-dependent refractive index of silicon and germanium," Proc. SPIE **6273**, 62732J (2006).
[97]M. Nedeljkovic, S. Stanković, C. J. Mitchell, A. Z. Khokhar *et al.*, "Mid-infrared thermo-optic modulators in SOI," IEEE Photonics Technol. Lett. **26**(13), 1352–1355 (2014).
[98]T. Fujigaki, S. Takagi, and M. Takenaka, "High-efficiency Ge thermo-optic phase shifter on Ge-on-insulator platform," Opt. Express **27**(5), 6451–6458 (2019).
[99]A. Malik, S. Dwivedi, L. Van Landschoot, M. Muneeb *et al.*, "Ge-on-Si and Ge-on-SOI thermo-optic phase shifters for the mid-infrared," Opt. Express **22**(23), 28479–28488 (2014).
[100]M. Nedeljkovic, R. Soref, and G. Z. Mashanovich, "Free-carrier electrorefraction and electroabsorption modulation predictions for silicon over the 1–14-μm infrared wavelength range," IEEE Photonics J. **3**(6), 1171–1180 (2011).
[101]M. Nedeljkovic, R. Soref, and G. Z. Mashanovich, "Predictions of free-carrier electroabsorption and electrorefraction in germanium," IEEE Photonics J. **7**(3), 1–14 (2015).
[102]W. Cao, D. Hagan, D. J. Thomson, M. Nedeljkovic *et al.*, "High-speed silicon modulators for the 2 μm wavelength band," Optica **5**(9), 1055–1062 (2018).
[103]X. Wang, W. Shen, W. Li, Y. Liu *et al.*, "High-speed silicon photonic Mach–Zehnder modulator at 2 μm," Photonics Res. **9**(4), 535–540 (2021).
[104]M. Nedeljkovic, C. G. Littlejohns, A. Z. Khokhar, M. Banakar *et al.*, "Silicon-on-insulator free-carrier injection modulators for the mid-infrared," Opt. Lett. **44**(4), 915–918 (2019).
[105]J. Leuthold, C. Koos, and W. Freude, "Nonlinear silicon photonics," Nat. Photonics **4**(8), 535–544 (2010).
[106]A. C. Turner, C. Manolatou, B. S. Schmidt, M. Lipson *et al.*, "Tailored anomalous group-velocity dispersion in silicon channel waveguides," Opt. Express **14**(10), 4357–4362 (2006).
[107]H. Fukuda, K. Yamada, T. Shoji, M. Takahashi *et al.*, "Four-wave mixing in silicon wire waveguides," Opt. Express **13**(12), 4629–4637 (2005).
[108]H. Rong, A. Liu, R. Jones, O. Cohen *et al.*, "An all-silicon Raman laser," Nature **433**(7023), 292–294 (2005).
[109]L. Yin, Q. Lin, and G. P. Agrawal, "Soliton fission and supercontinuum generation in silicon waveguides," Opt. Lett. **32**(4), 391–393 (2007).
[110]R. Halir, Y. Okawachi, J. S. Levy, M. A. Foster *et al.*, "Ultrabroadband supercontinuum generation in a CMOS-compatible platform," Opt. Lett. **37**(10), 1685–1687 (2012).
[111]Y. Zhang, K. Zhong, and H. K. Tsang, "Compact multimode silicon racetrack resonators for high-efficiency tunable Raman lasers," Appl. Phys. Lett. **122**(8), 081101 (2023).
[112]Q. Jin, T. Yin, Z. Tu, D. Chen *et al.*, "Performance evaluation of continuous-wave mid-infrared wavelength conversion in silicon waveguides," Appl. Opt. **58**(10), 2584–2588 (2019).
[113]R. K. W. Lau, M. Ménard, Y. Okawachi, M. A. Foster *et al.*, "Continuous-wave mid-infrared frequency conversion in silicon nanowaveguides," Opt. Lett. **36**(7), 1263–1265 (2011).

[114]S. Zlatanovic, J. S. Park, S. Moro, J. M. C. Boggio *et al.*, "Mid-infrared wavelength conversion in silicon waveguides using ultracompact telecom-band-derived pump source," Nat. Photonics **4**(8), 561–564 (2010).
[115]A. S. Kowligy, D. D. Hickstein, A. Lind, D. R. Carlson *et al.*, "Tunable mid-infrared generation via wide-band four-wave mixing in silicon nitride waveguides," Opt. Lett. **43**(17), 4220–4223 (2018).
[116]H. M. Pask, "The design and operation of solid-state Raman lasers," Prog. Quantum Electron. **27**(1), 3–56 (2003).
[117]M. Huang, S. Sun, T. S. Saini, Q. Fu *et al.*, "Raman amplification at 2.2 μm in silicon core fibers with prospects for extended mid-infrared source generation," Light: Sci. Appl. **12**(1), 209 (2023/08/2023).
[118]V. Raghunathan, D. Borlaug, R. R. Rice, and B. Jalali, "Demonstration of a mid-infrared silicon Raman amplifier," Opt. Express **15**(22), 14355–14362 (2007).
[119]V. M. N. Passaro and F. De Leonardis, "Investigation of SOI Raman lasers for mid-infrared gas sensing," Sensors **9**(10), 7814–7836 (2009).
[120]F. De Leonardis, B. Troia, R. A. Soref, and V. M. N. Passaro, "Investigation of germanium Raman lasers for the mid-infrared," Opt. Express **23**(13), 17237–17254 (2015).
[121]Z. Li, F. Han, Z. Dong, Q. Du, and Z. Luo, "On-chip mid-IR octave-tunable Raman soliton laser," Opt. Express **30**(14), 25356–25365 (2022).
[122]A. Zheng, Q. Sun, L. Wang, M. Liu *et al.*, "Impact of third-order dispersion and three-photon absorption on mid-infrared time magnification via four-wave mixing in $Si_{0.8}Ge_{0.2}$ waveguides," Appl. Opt. **59**(4), 1187–1192 (2020).
[123]N. Nader, A. Kowligy, J. Chiles, E. J. Stanton *et al.*, "Infrared frequency comb generation and spectroscopy with suspended silicon nanophotonic waveguides," Optica **6**(10), 1269–1276 (2019).
[124]A. Vasiliev, A. Malik, M. Muneeb, B. Kuyken *et al.*, "On-chip mid-infrared photothermal spectroscopy using suspended silicon-on-insulator microring resonators," ACS Sens. **1**(11), 1301–1307 (2016).
[125]B. Kuyken, T. Ideguchi, S. Holzner, M. Yan *et al.*, "An octave-spanning mid-infrared frequency comb generated in a silicon nanophotonic wire waveguide," Nat. Commun. **6**(1), 6310 (2015).
[126]A. G. Griffith, R. K. W. Lau, J. Cardenas, Y. Okawachi *et al.*, "Silicon-chip mid-infrared frequency comb generation," Nat. Commun. **6**(1), 6299 (2015).
[127]R. K. W. Lau, M. R. E. Lamont, A. G. Griffith, Y. Okawachi *et al.*, "Octave-spanning mid-infrared supercontinuum generation in silicon nanowaveguides," Opt. Lett. **39**(15), 4518–4521 (2014).
[128]L. Zhang, A. M. Agarwal, L. C. Kimerling, and J. Michel, "Nonlinear group IV photonics based on silicon and germanium: From near-infrared to mid-infrared," Nanophotonics **3**(4–5), 247–268 (2014).
[129]H. Guo, C. Herkommer, A. Billat, D. Grassani *et al.*, "Mid-infrared frequency comb via coherent dispersive wave generation in silicon nitride nanophotonic waveguides," Nat. Photonics **12**(6), 330–335 (2018).
[130]M. Yang, Y. Guo, J. Wang, Z. Han *et al.*, "Mid-IR supercontinuum generated in low-dispersion Ge-on-Si waveguides pumped by sub-ps pulses," Opt. Express **25**(14), 16116–16122 (2017).
[131]J. Yuan, Z. Kang, F. Li, X. Zhang *et al.*, "Mid-infrared octave-spanning supercontinuum and frequency comb generation in a suspended germanium-membrane ridge waveguide," J. Lightwave Technol. **35**(14), 2994–3002 (2017).
[132]J. Lai, J. Yuan, Y. Cheng, C. Mei *et al.*, "Dispersion-engineered T-type germanium waveguide for mid-infrared supercontinuum and frequency comb generations in all-normal dispersion region," OSA Continuum **3**(9), 2320–2331 (2020).
[133]G. Granger, M. Bailly, H. Delahaye, C. Jimenez *et al.*, "GaAs-chip-based mid-infrared supercontinuum generation," Light: Sci. Appl. **12**(1), 252 (2023).
[134]D. Weninger, S. S. Otálvaro, L. Ranno, L. Kimerling, and A. Agarwal, "Low loss chip-to-chip couplers for high density co-packaged optics," Optica Open (2024) https://doi.org/10.1364/opticaopen.25852735.v1.